ARTICLE

THE ANALYST
www.rsc.org/analyst

Identification of synthetic precursors of amphetamine-like drugs using Raman spectroscopy and *ab initio* calculations: β-Methyl-β-nitrostyrene derivatives

Nuno Milhazes,[a,b] Fernanda Borges,[a,c] Rita Calheiros[c] and M. Paula M. Marques*[c,d]

[a] *Departamento de Química Orgânica, Faculdade de Farmácia, Universidade do Porto, 4050-47 Porto, Portugal*

[b] *ISCS-Norte, Rua Central da Gandra, 1317, 4585-116 Gandra, PRD, Portugal*

[c] *Unidade I&D ''Química-Física Molecular'', Faculdade de Ciências e Tecnologia, Universidade de Coimbra, Ap. 3126, 3001-401 Coimbra, Portugal*

[d] *Departamento de Bioquímica, Faculdade de Ciências e Tecnologia, Universidade de Coimbra, Ap. 3126, 3001-401 Coimbra, Portugal. E-mail: pmc@ci.uc.pt*

Received 8th April 2004, Accepted 27th July 2004
First published as an Advance Article on the web 6th September 2004

The present work reports a vibrational spectroscopic study of several β-methyl-β-nitrostyrene derivatives, which are important intermediates in the synthesis of illicit amphetamine-like drugs, such as 3,4-methylenedioxymethamphetamine (MDMA), 3,4-methylenedioxyamphetamine (MDA), *p*-methoxyamphetamine (PMA) and 4-methylthioamphetamine (4-MTA). A complete conformational analysis of 3,4-methylenedioxy-β-methyl-β-nitrostyrene (3,4-MD-MeNS), 4-methoxy-β-methyl-β-nitrostyrene (4-MeO-MeNS), 4-methylthio-β-methyl-β-nitrostyrene (4-MeS-MeNS), was carried out by Raman spectroscopy coupled to *ab initio* MO calculations—both complete geometry optimisation and harmonic frequency calculation. The Raman spectra show characteristic features of these precursors, which allow their ready differentiation and identification. It was verified that the conformational behaviour of these systems is mainly determined by the stabilising effect of π-electron delocalisation.

1 Introduction

Nitroalkenes in general, and β-nitrostyrene derivatives in particular, are very versatile compounds in synthetic organic chemistry, namely as starting materials for the synthesis of a variety of useful building blocks such as nitroalkanes, amines, ketoximes, hydroxylamines and aldoximes.[1–3] Conjugated nitroalkenes are especially reactive, since they are excellent Michael acceptors both to organometallic reagents[4] and ascorbic acid.[5]

The illegal manufacture of amphetamine-like drugs of abuse relies upon the preparation of the appropriate β-methyl-β-nitrostyrene precursors, *via* Knoevenagel-type condensation. This route is one of the synthetic pathways used in the preparation of the following recreational drugs: 3,4-methylenedioxymethamphetamine (''ecstasy'' or MDMA), 3,4-methylenedioxyamphetamine (MDA), 4-methylthioamphetamine (MTA) and 4-methoxyamphetamine (PMA).[6] The abuse of psychoactive drugs such as the above mentioned ones is known to produce serious health problems in users, which can even result in death. While there has been much research on the effect of these drugs in humans, little has been investigated on the effect of the side products and synthetic reaction by-products. β-Nitrostyrene, an intermediate of amphetamine synthesis, has been shown to affect both cell viability and macrophage function.[7] Thus, ingestion of nitrostyrene-contaminated drugs of abuse (*e.g.* ''ecstasy'') is likely to have a considerable adverse effect on the user (namely on their immune response).[7]

Since different synthetic precursors and intermediates are usually found in illegally produced drugs of abuse,[8] the determination of their presence in these products, as well as their thorough characterisation, is of considerable forensic interest as a means of tracking the clandestine laboratories engaged in the production of such drugs. In addition it could be an important tool for the knowledge of the toxicity profile of the drugs.

Raman spectroscopy has proved, in the last few years, to be a simple and reliable method for the determination of the composition profile of solid samples (*e.g.* seized ''ecstasy'' tablets).[9–13] Actually, due to its non-invasiveness, high sensitivity and good reproducibility, apart from the fact that it needs virtually no sample preparation, this technique is presently becoming an important tool for the screening of illicit drugs in forensic laboratories, once it yields unique fingerprint spectra, specific for each compound. Moreover the method can be applied either for pure compounds or mixtures.

Reports dealing with the identification of specific synthetic markers of amphetamine-like drugs are scarce. Although several synthetic routes are usually followed (Fig. 1), namely the Leuckart method, the nitrostyrene route used in the present study is also a routine strategy, yielding intermediates with a high cytoxicity (unpublished data). The present work reports the spectral characterisation, through Raman spectroscopy, of the following synthetic precursors of amphetamine-like drugs: 3,4-methylenedioxy-β-methyl-β-nitrostyrene (3,4-MD-MeNS), 4-methoxy-β-methyl-β-nitrostyrene (4-MeO-MeNS) and 4-methylthio-β-methyl-β-nitrostyrene (4-MeS-MeNS). A complete conformational analysis of these compounds was also performed by *ab initio* MO methods—both complete geometry optimisation and harmonic frequency calculation—thus allowing a thorough assignment of the experimental spectral features. The results thus obtained will, in the future, allow a rapid and unequivocal spectroscopic identification of these synthetic precursors of illegally produced drugs of abuse.

2 Materials and methods

2.1 Synthesis

The synthesis of each β-methyl-β-nitrostyrene was performed as described in a recent paper,[14] using nitroethane and the

DOI: 10.1039/b405290k

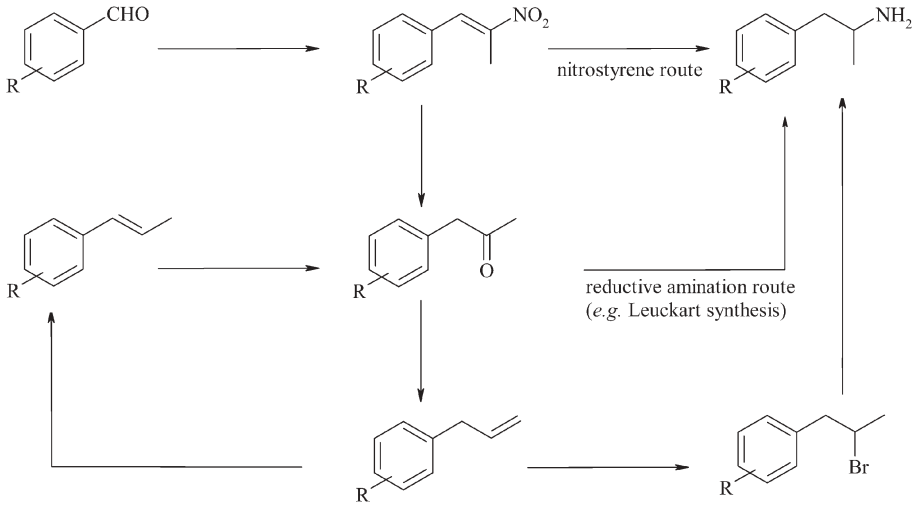

Fig. 1 Schematic representation of the general synthetic routes for amphetamine-like drugs.

benzaldehyde with the corresponding aromatic substitution pattern (Fig. 1). The synthesised compounds were identified by both NMR and electron impact mass spectroscopy (EI-MS).

3,4-Methylenedioxy-*β*-methyl-*β*-nitrostyrene (3,4-MD-MeNS). Yield 91%; ^{1}H NMR δ: 2.40 (3H, s, CH_3), 6.12 (2H, s, CH_2), 7.06 (1H, d, J = 8.1, H(5)), 7.18 (1H, dd, J = 8.2; 1.6, H(6)), 7.22 (1H, d, J = 1.6, H(2)), 8.04 (1H, s, H(α)); ^{13}C NMR δ: 14.0 CH_3, 101.9 CH_3, 108.8 *C*HAr, 109.8 *C*HAr, 125.9 C(1), 126.4 *C*HAr, 133.4 C(α), 146.0 C(β), 147.8 C(3), 149.1 C(4); EI-MS *m*/*z* (%): 207 ($M^{+\bullet}$, 100), 160 (82), 131 (18), 77 (49); mp 91–92 °C.

4-Methoxy-*β*-methyl-*β*-nitrostyrene (4-MeO-MeNS). Yield 84%; ^{1}H NMR δ: 2.42 (3H, s, CH_3), 3.83 (3H, s, OCH_3), 7.07 (2H, d, J = 8.8, H(3) and (5)), 7.60 (2H, d, J = 8.4, H(2) and H(6)), 8.08 (1H, s, H(α)); ^{13}C NMR δ: 13.9 *C*H_3, 55.4 O*C*H_3, 114.5 (2C, C(3) and C (5)), 124.3 C(1), 132.5 (2C, C(2) and C (6)), 133.3 C(α), 145.4 C(β), 160.9 C(4); EI-MS *m*/*z* (%): 193 ($M^{+\bullet}$, 85), 146 (100), 131 (44), 115 (49), 103 (57), 91 (44), 77 (43), 63 (23); mp 40–43 °C.

4-Methylthio-*β*-methyl-*β*-nitrostyrene (4-MeS-MeNS). Yield 67%; ^{1}H NMR δ: 2.42 (3H, s, CH_3), 2.53 (3H, *s*, SCH_3), 7.36 (2H, d, J = 8.4, H(3) and (5)), 7.55 (2H, d, J = 8.4, H(2) and H(6)), 8.07 (1H, s, H(α)); ^{13}C NMR δ: 14.1 *C*H_3, 14.1 S*C*H_3, 125.5 (2C, C(3) and C (5)), 128.2 C(1), 131.0 (2C, C(2) and C (6)), 133.0 C(α), 142.0 C(β), 146.8 C(4); EI-MS *m*/*z* (%): 209 ($M^{+\bullet}$, 100), 162 (78), 147 (41), 132 (24), 115 (95), 103 (18), 89 (19), 77 (19), 63 (21); mp 69–70 °C.

2.2 Apparatus

^{1}H and ^{13}C NMR data were acquired at room temperature, on a Brüker AMX 300 spectrometer operating at 300.13 and 75.47 MHz, respectively. Dimethylsulfoxide-d_6 was used as a solvent. Chemical shifts are expressed in δ (ppm) values relative to tetramethylsilane (TMS) as an internal reference; coupling constants (J) are given in Hz. Assignments were also made from DEPT (distortionless enhancement by polarization transfer) (underlined values). EI-MS was carried out on a VG AutoSpec instrument; the data are reported as *m*/*z* (% of relative intensity of the most important fragments). Melting points were obtained on a Köfler microscope (Reichert Thermovar) and are uncorrected.

2.3 *Ab initio* MO calculations

The *ab initio* molecular orbital calculations—full geometry optimisation and calculation of the harmonic vibrational frequencies—were performed using the GAUSSIAN 98W program,[15] within the Density Functional Theory (DFT) approach in order to properly account for the electron correlation effects (particularly important in this kind of conjugated system). The widely employed hybrid method denoted by B3LYP,[16–21] which includes a mixture of HF and DFT exchange terms and the gradient-corrected correlation functional of Lee, Yang and Parr,[22,23] as proposed and parameterised by Becke,[24,25] was used, along with the double-zeta split valence basis set 6–31G**.[26,27] All frequency calculations were run at the B3LYP/6-31G** level, and wavenumbers above 400 cm^{-1} were scaled[28] before comparing them with the experimental data.

Molecular geometries were fully optimised by the Berny algorithm, using redundant internal coordinates:[29] The bond lengths to within *ca.* 0.1 pm and the bond angles to within *ca.* 0.1°. The final root-mean-square (rms) gradients were always less than 3×10^{-4} E_h a_0^{-1} or E_h rad^{-1}. No geometrical constraints were imposed on the molecules under study.

2.4 Spectroscopic methods

The Raman spectra were obtained at room temperature, on a triple monochromator Jobin-Yvon T64000 Raman system (0.640 m, *f*/7.5), with holographic gratings of 1800 grooves mm^{-1}. The detection system was a non-intensified CCD (Charge Coupled Device). The entrance slit was set to 200 μm and the slit between the premonochromator and the spectrograph was opened to 14.0 mm. The 514.5 nm line of an Ar^+ laser (Coherent, model Innova 300) was used as the excitation radiation, providing between 10 to 90 mW at the sample position. Under the above mentioned conditions, the error in wavenumbers was estimated to be within 1 cm^{-1}.

Room-temperature FT-Raman spectra were recorded on an RFS-100 Bruker FT-spectrometer, using an Nd:YAG laser with an excitation wavelength of 1064 nm. Each spectrum is the average of two repeated measurements of 150 scans each, at a 2 cm^{-1} resolution. In all experiments, the samples were sealed in Kimax glass tubes of 0.8 mm inner diameter.

2.5 Chemicals

4-Methoxybenzaldehyde, 4-methylthiobenzaldehyde, 3,4-methylenedioxybenzaldehyde, ammonium acetate and nitroethane were obtained from Sigma-Aldrich Química S.A. (Sintra, Portugal). All other reagents and solvents were *pro analysis* grade, purchased from Merck (Lisbon, Portugal).

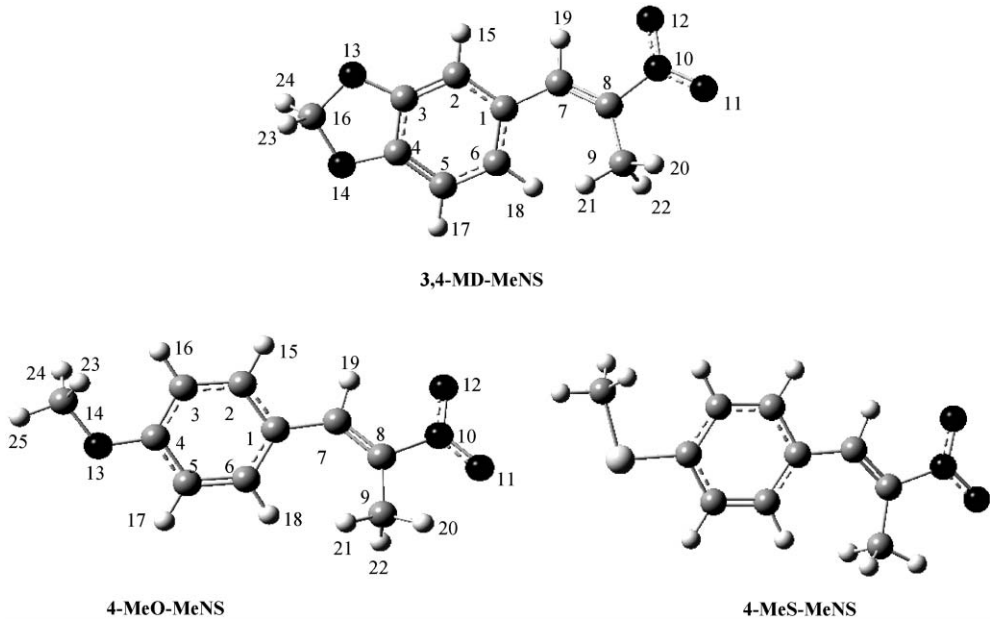

Fig. 2 Most stable conformers for the precursors of amphetamine-like drugs studied in the present work (at the B3LYP/6-31G** level of calculation. The atom numbering is included).

3 Results and discussion

3.1 *Ab initio* MO calculations

A complete geometry optimisation was carried out for the three β-methyl-β-nitrostyrene derivatives studied: 3,4-methylenedioxy-β-methyl-β-nitrostyrene (3,4-MD-MeNS), 4-methoxy-β-methyl-β-nitrostyrene (4-MeO-MeNS) and 4-methylthio-β-methyl-β-nitrostyrene (4-MeS-MeNS) (Fig. 2). The effect of several structural parameters on the overall stability of these compounds was investigated, namely: (i) orientation of both the aromatic ring and the NO_2 group relative to the C_7=C_8 bond—($C_1C_7C_8N_{10}$) dihedral equal to 0° or 180°, defining either a *Z* or an *E* configuration, respectively; (ii) position of the CH_3 and NO_2 groups relative to the ring—($C_2C_1C_7C_8$) dihedral either 0° or 180°.

3,4-Methylenedioxy-β-methyl-β-nitrostyrene. Four different conformers were calculated for 3,4-MD-MeNS, the most stable ones displaying an *E* orientation of both the aromatic ring and the terminal nitro group relative to the C_7=C_8 bond—conformers 1 ($\Delta E = 0$) and 2 ($\Delta E = 0.6$ kJ mol^{-1}) (Fig. 3), with populations at room temperature of 59% and 41%, respectively. In fact, the geometries with a dihedral ($C_1C_7C_8N_{10}$) $\approx 180°$ were found to be highly favoured relative to the ones displaying a *Z* conformation (($C_1C_7C_8N_{10}$) = 0°)—3,4-MD-MeNS 3 ($\Delta E = 19.4$ kJ mol^{-1}) and 4 ($\Delta E = 22.0$ kJ mol^{-1}) (Fig. 3)—most probably due to a more effective π-electron delocalisation, as well as to a minimisation of steric repulsions. Moreover, the large energy difference between conformations 1 and 3 ($\Delta E = 19.4$ kJ mol^{-1}), or 2 and 4 ($\Delta E = 21.4$ kJ mol^{-1}), is solely due to the change in the ($C_1C_7C_8N_{10}$) dihedral angle

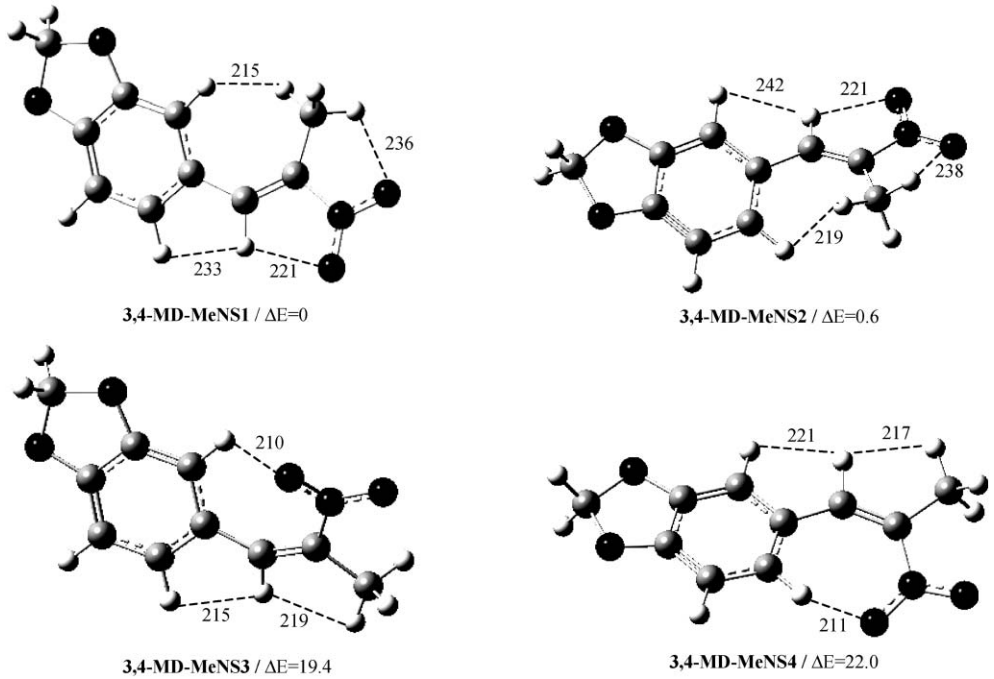

Fig. 3 Schematic representation of the calculated (B3LYP/6-31G**) conformers for 3,4-MD-MeNS. (Intramolecular hydrogen bonds are shown. Distances in pm; relative energies in kJ mol^{-1}).

from 180° to 0°, which leads to stronger steric repulsions between H_{18} and H_{19} in conformer 3 ($H_{18}\cdots H_{19}$ of 215 pm), or H_{15} and H_{19} in conformer 4 ($H_{15}\cdots H_{19}$ of 221 pm), relative to the *E* conformers. In addition, the greater stability of 3,4-MD-NeNS 1 and 2 can be explained by the formation of a medium strength intramolecular H-bond between H_{20} (methyl group) and O_{11} (NO_2 group), (C)H···O(N) distance being equal to 236 and 238 pm, respectively (Fig. 3), which does not occur in the *Z* conformations.

A higher deviation of the side carbon chain relative to the aromatic ring was detected for those geometries displaying an *E* conformation—3,4-MD-MeNS 1 (($C_2C_1C_7C_8$) = −23.5°) and 3,4-MD-MeNS 2 (($C_2C_1O_7C_8$) = 154.4°)—relative to the *Z* conformers—3,4-MD-MeNS 3 (($C_2C_1O_7C_8$) = 12.5°) and 3,4-MD-MeNS 4 (($C_2C_1O_7C_8$) = −165.7°). This is due to steric hindrance effects between H atoms from the CH_3 group and the aromatic ring (H···H intramolecular distances between 215 and 219 pm), which can only occur in the *E* isomers. The NO_2 group displays a clear preference for planarity (dihedrals ($C_1C_7C_8N_{10}$) and ($C_7C_8N_{10}O_{11}$) around 177° in conformers 1 and 2, Table 1), once it allows a more effective electron delocalisation between the aromatic ring, the C=C double bond and the terminal NO_2.

As expected for this kind of compound, the most stable conformers were found to display a slight deviation from planarity relative to the aromatic ring of both the methylenedioxy group (($C_2C_3O_{13}C_{16}$) = 176.9°; ($C_3O_{13}C_{16}O_{14}$) = 7.0°, Table 1) and the carbon side chain (($C_2C_1C_7C_8$) = −23.5°; ($C_1C_7C_8C_9$) = −4.4°, Table 1), on account of the steric hindrance occurring between hydrogen atoms within the molecule (*e.g.* $H_{15}\cdots H_{21}$ and $H_{15}\cdots H_{21}$, H···H distances equal to 215 and 233 pm, respectively).

4-Methoxy-*β*-methyl-*β*-nitrostyrene and 4-methylthio-*β*-methyl-*β*-nitrostyrene. Four stable geometries were calculated for both 4-MeO-MeNS and 4-MeS-MeNS, but only the *E* conformers, 1 ($\Delta E = 0$) and 2 ($\Delta E = 0.3$ kJ mol^{-1}), were found to be significantly populated at room temperature—53% and 47%, respectively, for both compounds (Fig. 4). As previously discussed for 3,4-MD-MeNS, the higher stability of the *E* conformations is easily explained by an effective π-electron delocalisation (which is favoured for this geometry), along with the formation of a stabilising intramolecular H-bond between H_{20} (CH_3 group) and O_{11} (NO_2 group), with a (C)$H_{20}\cdots O_{11}$(N) distance between 236 and 238 pm (Fig. 4).

For these two *para* substituted nitrostyrenes, the *Z* conformations—4-MeO-MeNS 3 (ΔE = 19.2 kJ mol^{-1}) and 4 (ΔE = 20.0 kJ mol^{-1}), 4-MeS-MeNS 3 (ΔE = 19.3 kJ mol^{-1}) and 4 (ΔE = 20.0 kJ mol^{-1})—were found to be highly unfavourable relative to the *E* ones, probably due to repulsive effects coupled to a less effective π-electron delocalisation. In fact, the *Z* conformers display strong intramolecular repulsions between atoms H_{15} and H_{19} ($H_{15}\cdots H_{19}$ distance between 217 and 218 pm), or H_{18} and H_{19} ($H_{18}\cdots H_{19}$ distance between 217 and 219 pm), which leads to a lower stabilisation. Moreover, in these *Z* isomers there is a slightly larger deviation of the nitro group relative to the carbon chain, resulting in a less effective π-electron delocalisation within the molecule and consequently to higher relative conformational energies—*e.g.* 4-MeO-MeNS 1 (($C_1C_7C_8N_{10}$) = 177.3°, ($C_7C_8N_{10}O_{11}$) = −177.2°)) *vs.* 4-MeO-MeNS 3 (($C_1C_7C_8N_{10}$) = 5.1°, ($C_7C_8N_{10}O_{11}$) = −169.8°)), and 4-MeS-MeNS 1 (($C_1C_7C_8N_{10}$) = 175.5°, ($C_7C_8N_{10}O_{11}$) = −177.2°)) *vs.* 4-MeS-MeNS 3 (($C_1C_7C_8N_{10}$) = −5.4°, ($C_7C_8N_{10}O_{11}$) = 166.4°)) (Fig. 4).

For all energy minima, the OMe and SMe groups were found to be planar or *quasi*-planar relative to the aromatic ring (($C_3C_4O_{13}C_{14}$) = −0.2°, ($C_3C_4S_{13}C_{14}$) = 0.3°, Tables 2 and 3). The atoms H_{23} and H_{24} from the CH_3 group are thus equidistant to H_{16}, leading to a minimisation of H···H steric repulsions.

Table 1 Calculated geometrical parameters (B3LYP/6-31G**) for the most stable conformers of 3,4-MD-MeNS

[a](ΔE/kJ mol^{-1})/([b] μ/D)	3,4-MD-MeNS 1 0.0/6.3	3,4-MD-MeNS 2 0.9/6.2
Bond lengths/pm		
[c]C_1–C_2	142.1	142.2
C_2–C_3	137.6	137.5
C_3–C_4	139.6	139.5
C_4–C_5	138.2	138.2
C_5–C_6	140.1	140.3
C_6–C_1	140.9	140.7
C_1–C_7	145.9	146.1
C_7–C_8	134.9	134.8
C_8–C_9	149.6	149.6
C_3–O_{13}	137.3	137.2
C_4–O_{14}	136.7	136.7
C_{16}–O_{13}	143.2	143.3
C_{16}–O_{14}	143.6	143.7
C_8–N_{10}	148.0	148.1
N_{10}–O_{11}	123.4	123.4
N_{10}–O_{12}	123.3	123.3
C_2–H_{15}	108.1	108.4
C_5–H_{17}	108.3	108.4
C_6–H_{18}	108.5	108.2
C_{16}–H_{23}	109.4	109.6
C_{16}–H_{24}	109.8	109.6
C_7–H_{19}	108.6	108.6
C_9–H_{20}	109.1	109.1
C_9–H_{21}	109.1	109.1
C_9–H_{22}	109.6	109.6
Bond angles/degrees		
C_6–C_1–C_2	119.3	119.4
C_6–C_1–C_7	117.0	123.7
C_1–C_7–C_8	129.9	129.5
C_7–C_8–C_9	130.2	130.0
C_4–C_3–O_{13}	109.5	109.6
C_3–O_{13}–C_{16}	106.1	106.2
C_7–C_8–N_{10}	115.6	115.7
C_8–N_{10}–O_{11}	116.6	116.6
O_{11}–N_{10}–O_{12}	123.8	123.8
C_8–C_7–H_{19}	114.6	114.8
C_8–C_9–H_{20}	110.0	110.1
C_8–C_9–H_{21}	110.2	110.0
H_{20}–C_9–H_{21}	109.0	109.3
H_{20}–C_9–H_{22}	106.7	106.7
H_{23}–C_{16}–H_{24}	111.0	110.9
Dihedral angles/degrees		
C_1–C_2–C_3–C_4	0.3	−1.3
C_3–C_2–C_1–C_7	179.9	179.9
C_2–C_1–C_7–C_8	−23.5	154.4
C_1–C_7–C_8–C_9	−4.4	−4.4
C_1–C_7–C_8–N_{10}	177.3	177.5
C_7–C_8–N_{10}–O_{11}	−177.4	−177.7
C_2–C_3–O_{13}–C_{16}	176.9	−179.7
C_3–O_{13}–C_{16}–O_{14}	7.1	−1.7
C_3–O_{13}–C_{16}–H_{23}	126.0	117.4
C_3–O_{13}–C_{16}–H_{24}	−111.9	−120.7
C_6–C_1–C_2–H_{15}	175.5	−178.7
C_3–C_4–C_5–H_{17}	178.9	−178.3
C_4–C_5–C_6–H_{18}	179.8	−177.4
C_6–C_1–C_7–H_{19}	−20.7	153.5
C_7–C_8–C_9–H_{20}	−141.3	−139.8
C_7–C_8–C_9–H_{21}	−21.1	−19.3

[a] Total value of energy for the most stable conformer of 3,4-MD-MeNS is −703.925705439 E_h (1 E_h = 2625.5001 kJ mol^{-1}). [b] D = 1/3 × 10^{-2} C m. [c] Atoms are numbered according to Fig. 2.

3.2 Raman spectroscopy

The Raman spectra of the drug precursors investigated in this work (solid state) are represented in Fig. 5, for both the 75–1750 cm^{-1} and 2200–3400 cm^{-1} regions. Experimental Raman wavenumbers for 3,4-MD-MeNS, 4-MeO-MeNS and

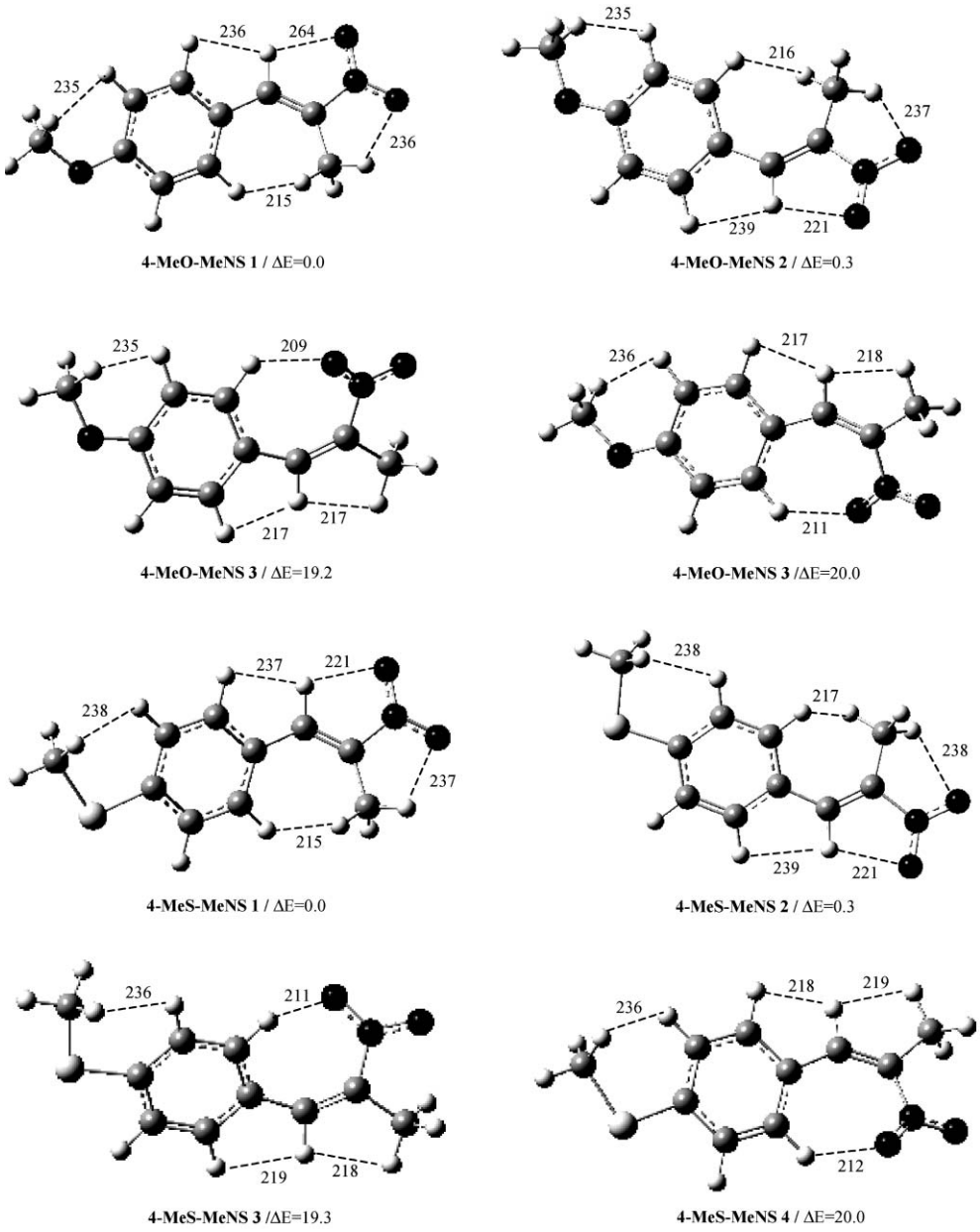

Fig. 4 Schematic representation of the calculated (B3LYP/6-31G**) conformers for 4-MeO-MeNS and 4-MeS-MeNS. (Intramolecular hydrogen bonds are shown. Distances in pm; relative energies in kJ mol^{-1}.)

4-MeS-MeNS are listed in Tables 4, 5 and 6, respectively, along with the calculated values for the two most stable conformers found for each compound.

A complete assignment of the experimental vibrational features was carried out (Tables 4 to 6), in the light of both the theoretical results presently performed and the spectroscopic data previously reported for *β*-methyl-*β*-nitrostyrene derivatives[14,30,31] and similar systems.[32–38]

The main Raman spectral features common to all compounds studied were (Fig. 5): (i) the C=C ring stretching vibrations, at *ca.* 1515–1645 cm^{-1} and 1220–1390 cm^{-1}; the in-plane and out-of-plane C=C ring deformations, respectively around 630–1100 cm^{-1} and 425–717 cm^{-1}; the out-of-plane C=C ring deformation, at *ca.* 717 cm^{-1}, which was often found to be overlapped with the NO_2 wagging mode; (ii) the linear chain C=C stretching vibrations, at *ca.* 1646–1650 cm^{-1}; (iii) the NO_2 symmetric and antisymmetric stretching modes, at *ca.* 1300 cm^{-1} and *ca.* 1550 cm^{-1}, respectively; the NO_2 scissoring modes at *ca.* 830–880 cm^{-1}; (iv) The CH_3 symmetric and antisymmetric stretching modes, respectively around 2907–2987 cm^{-1} and 2976–3045 cm^{-1}, along with the other CH stretching vibrations between 3000 cm^{-1} and 3250 cm^{-1}.

The Raman band due to the symmetric stretching of the nitro group, detected at *ca.* 1300 cm^{-1}, is the most intense one in all the spectra presently recorded (Fig. 5). In turn, relatively intense bands at *ca.* 1310 cm^{-1} and 1605 to 1641 cm^{-1}—assigned to $\nu\ (C{=}C)_{ring}$—are often overlapped with both $\nu_s\ (NO_2)$ (at *ca.* 1298 to 1316 cm^{-1}) and $\nu\ (C{=}C)_{chain}$ (at *ca.* 1650 cm^{-1}), respectively (Tables 4 to 6). Moreover, the moderately intense bands detected between 1170 and 1260 cm^{-1}, associated to the C–H in-plane ring deformations, were easily detected for all three nitrostyrenes studied. The Raman spectra of these compounds also yield typical features of the methyl group, namely $\delta_s\ (CH_3)_{chain}$ (1355 to 1365 cm^{-1}), $\delta_{as}\ (CH_3)_{chain}$ (1434 to 1452 cm^{-1}) and $\tau\ (CH_3)_{chain}$ (218 to 303 cm^{-1}), the latter with very low intensity (Tables 4 to 6).

Despite the common vibrational features, the *β*-methyl-*β*-nitrostyrene derivatives under study were found to give rise to distinctive Raman patterns, which allow them to be easily

Table 2 Calculated geometrical parameters (B3LYP/6-31G**) for the most stable conformers of 4-MeO-MeNS

[a](ΔE/kJ mol^{-1})/[b](μ/D)	4-MeO-MeNS 1 0.0/6.7	4-MeO-MeNS 2 0.3/6.8
Bond lengths/pm		
[c]C_1–C_2	140.7	140.6
C_2–C_3	139.1	139.3
C_3–C_4	140.2	140.2
C_4–C_5	140.5	140.5
C_5–C_6	138.4	138.3
C_6–C_1	141.3	141.3
C_1–C_7	145.8	145.9
C_7–C_8	134.9	134.9
C_8–C_9	149.6	149.6
C_4–O_{13}	135.8	135.8
O_{13}–C_{14}	142.2	142.2
C_8–N_{10}	147.9	147.9
N_{10}–O_{11}	123.4	123.4
N_{10}–O_{12}	123.3	123.3
C_2–H_{15}	108.5	108.3
C_3–H_{16}	108.3	108.3
C_5–H_{17}	108.5	108.5
C_6–H_{18}	108.3	108.6
C_7–H_{19}	108.6	108.6
C_9–H_{20}	109.1	109.1
C_9–H_{21}	109.1	109.1
C_9–H_{22}	109.6	109.6
C_{14}–H_{23}	109.8	109.7
C_{14}–H_{24}	109.7	109.7
C_{14}–H_{25}	109.0	109.0
Bond angles/degrees		
C_6–C_1–C_2	117.3	117.3
C_6–C_1–C_7	124.9	117.9
C_1–C_7–C_8	129.8	129.6
C_7–C_8–C_9	129.9	129.9
C_4–O_{13}–C_{14}	118.5	118.6
C_7–C_8–N_{10}	115.7	115.8
C_8–N_{10}–O_{11}	116.6	116.6
O_{11}–N_{10}–O_{12}	123.7	123.8
O_{13}–C_{14}–H_{23}	111.5	111.5
O_{13}–C_{14}–H_{24}	111.5	111.5
C_1–C_2–H_{15}	118.9	120.0
C_2–C_3–H_{16}	119.5	119.2
C_8–C_7–H_{19}	114.6	114.7
C_8–C_9–H_{20}	110.1	110.1
C_8–C_9–H_{21}	110.1	110.0
H_{20}–C_9–H_{21}	109.1	109.2
H_{20}–C_9–H_{22}	106.8	106.8
H_{23}–C_{14}–H_{24}	109.3	109.3
H_{23}–C_{14}–H_{25}	109.3	109.3
Dihedral angles/degrees		
C_1–C_2–C_3–C_4	−1.3	−0.1
C_3–C_2–C_1–C_7	−179.6	−179.5
C_2–C_1–C_7–C_8	158.3	−25.7
C_1–C_7–C_8–C_9	−4.3	−4.4
C_1–C_7–C_8–N_{10}	177.3	177.3
C_7–C_8–N_{10}–O_{11}	−177.2	−177.7
C_2–C_3–C_4–O_{13}	−179.6	179.6
C_3–C_4–O_{13}–C_{14}	−0.2	0.7
C_6–C_1–C_2–H_{15}	−178.5	175.8
C_1–C_2–C_3–H_{16}	179.2	179.2
C_3–C_4–C_5–H_{17}	−178.2	179.0
C_4–C_5–C_6–H_{18}	−177.7	179.5
C_6–C_1–C_7–H_{19}	157.4	−22.2
C_7–C_8–C_9–H_{20}	−141.8	−140.5
C_7–C_8–C_9–H_{21}	−21.5	−20.1
C_4–O_{13}–C_{14}–H_{23}	−61.2	−62.0
C_4–O_{13}–C_{14}–H_{24}	61.2	60.4

[a] Total value of energy for the most stable conformer of 4-MeO-MeNS is −668.009740128 E_h (1 E_h = 2625.5001 kJ mol^{-1}). [b] D = 1/3 × 10^{-2} C m. [c] Atoms are numbered according to Fig. 2.

Table 3 Calculated geometrical parameters (B3LYP/6-31G**) for the most stable conformers of 4-MeS-MeNS

[a](ΔE/kJ mol^{-1})/[b](μ/D)	4-MeS-MeNS 1 0.0/6.1	4-MeS-MeNS 2 0.3/7.3
Bond lengths/pm		
[c]C_1–C_2	140.7	140.7
C_2–C_3	139.0	139.2
C_3–C_4	140.2	140.2
C_4–C_5	140.6	140.7
C_5–C_6	138.6	138.5
C_6–C_1	141.3	141.1
C_1–C_7	145.9	146.9
C_7–C_8	134.8	134.8
C_8–C_9	149.6	149.6
C_4–S_{13}	177.5	177.5
S_{13}–C_{14}	182.2	182.2
C_8–N_{10}	148.1	148.0
N_{10}–O_{11}	123.4	123.4
N_{10}–O_{12}	123.3	123.3
C_2–H_{15}	108.6	108.3
C_3–H_{16}	108.3	108.4
C_5–H_{17}	108.6	108.6
C_6–H_{18}	108.3	108.6
C_7–H_{19}	108.6	108.6
C_9–H_{20}	109.1	109.1
C_9–H_{21}	109.1	109.1
C_9–H_{22}	109.6	109.6
C_{14}–H_{23}	109.2	109.2
C_{14}–H_{24}	109.2	109.2
C_{14}–H_{25}	109.2	109.2
Bond angles/degrees		
C_6–C_1–C_2	117.3	117.3
C_6–C_1–C_7	124.9	117.9
C_1–C_7–C_8	129.7	129.4
C_7–C_8–C_9	130.0	129.9
C_4–S_{13}–C_{14}	103.8	103.8
C_7–C_8–N_{10}	115.7	115.9
C_8–N_{10}–O_{11}	116.6	116.6
O_{11}–N_{10}–O_{12}	123.8	123.9
S_{13}–C_{14}–H_{23}	111.5	111.5
S_{13}–C_{14}–H_{24}	111.6	111.5
C_2–C_3–H_{15}	118.9	120.0
C_2–C_3–H_{16}	119.0	118.7
C_8–C_7–H_{19}	114.7	114.8
C_8–C_9–H_{20}	110.1	110.0
C_8–C_9–H_{21}	110.1	110.1
H_{20}–C_9–H_{21}	109.1	109.2
H_{20}–C_9–H_{22}	106.8	106.8
H_{23}–C_{14}–H_{24}	110.4	110.4
H_{23}–C_{14}–H_{25}	108.9	108.9
Dihedral angles/degrees		
C_1–C_2–C_3–C_4	−1.3	−0.1
C_3–C_2–C_1–C_7	−179.5	−179.5
C_2–C_1–C_7–C_8	157.2	−26.4
C_1–C_7–C_8–C_9	−4.1	−4.3
C_1–C_7–C_8–N_{10}	177.5	177.4
C_7–C_8–N_{10}–O_{11}	−177.2	−177.6
C_2–C_3–C_4–S_{13}	−179.8	−179.5
C_3–C_4–S_{13}–C_{14}	0.3	0.5
C_6–C_1–C_2–H_{15}	−178.5	175.8
C_1–C_2–C_3–H_{16}	179.1	179.2
C_3–C_4–C_5–H_{17}	−178.2	179.0
C_4–C_5–C_6–H_{18}	−177.7	179.5
C_6–C_1–C_7–H_{19}	156.5	−22.9
C_7–C_8–C_9–H_{20}	−141.0	−139.8
C_7–C_8–C_9–H_{21}	−20.7	−19.4
C_4–S_{13}–C_{14}–H_{23}	111.5	111.5
C_4–S_{13}–C_{14}–H_{24}	−61.9	−62.3

[a] Total value of energy for the most stable conformer of 4-MeS-MeNS is −990.987429241 E_h (1 E_h = 2625.5001 kJ mol^{-1}). [b] D = 1/3 × 10^{-2} C m. [c] Atoms are numbered according to Fig. 2, irrespective of the type of atom (O or S).

identified through this spectroscopic technique. 3,4-MD-MeNS is characterised by the frequencies at 1201 cm^{-1} (t (CH_2), 1034 cm^{-1}, (δ (OCO) and δ ($CH)_{ring}$) and 945 cm^{-1} (ν ($C_{16}O$)). MeO-MeNS and 4-MeS-MeNS, in turn, are readily identified by the medium intensity bands due to the ϕ-O and ϕ-S stretching modes detected at 1256 and 1095 cm^{-1}, respectively, as well as by the low intensity features observed at 1037 and

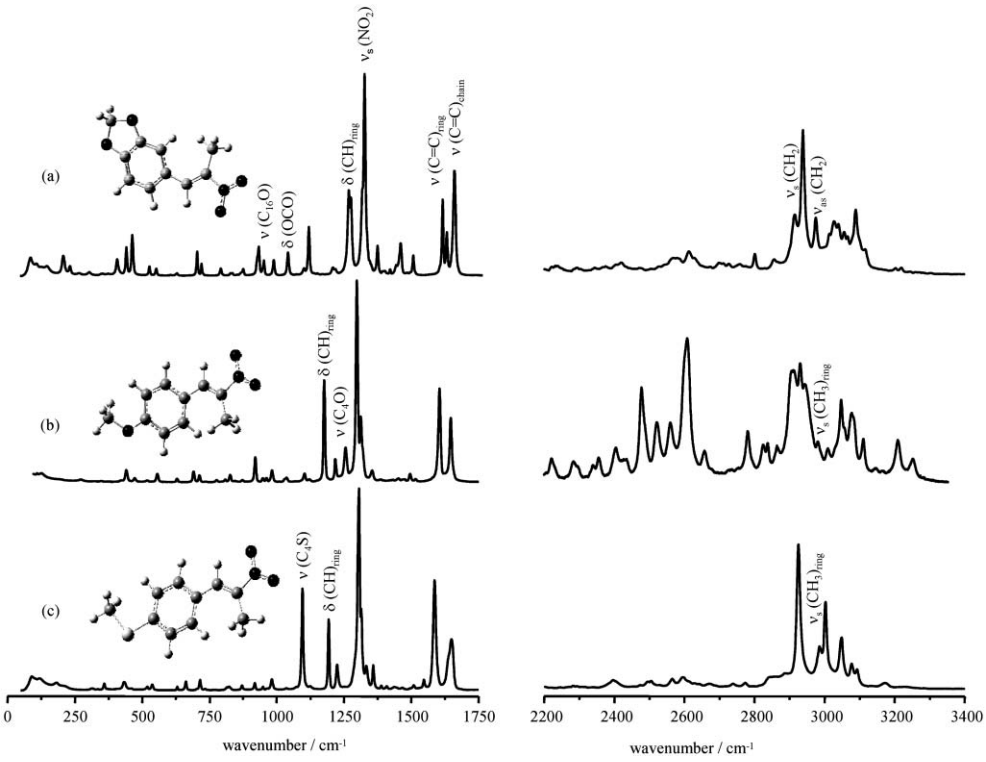

Fig. 5 Experimental Raman spectra (75–1750 cm^{-1} and 2200–3400 cm^{-1}) in the solid state (at 25 °C) for some of the precursors of amphetamine-like drugs studied in the present work: (a) 3,4-MD-MeNS (FT-Raman); (b) 4-MeO-MeNS; (c) 4-MeS-MeNS (FT-Raman).

662 cm^{-1}, ascribed to ν (C_4O) and ν (C_4S), respectively (Fig. 5, Tables 5 and 6).

When comparing the results reported for *β*-methyl-*β*-nitrostyrene (MeNS)[14] with the ones now obtained for compounds 4-MeO-MeNS and 4-MeS-MeNS, it is evident that the presence of a *para* substituent in the aromatic ring (either O–CH_3 or S–CH_3) has a strong effect on both the CH_3 and NO_2 vibrational modes: $\delta_s(CH_3)_{chain}$ is shifted to lower frequency values relative to the ones measured for MeNS (1385 cm^{-1})—$\Delta\nu \approx 30$ cm^{-1} for 4-MeO-MeNS and $\Delta\nu \approx 26$ cm^{-1} for 4-MeS-MeNS, while ν_s (NO_2) displays a shift from 1316 cm^{-1} to 1298 or 1306 cm^{-1}, respectively for OCH_3 and SCH_3 substitutions.

Indeed, for these *para* substituted compounds it was found that an O → S substitution leads to a quite large downward shift of the C–O and C–S stretching modes: a deviation of 161 cm^{-1} was obtained for ν ($C_{14}O$) and ν ($C_{14}S$), while a 375 cm^{-1} shift was determined for ν (C_4O) and ν (C_4S) (Fig. 5, Tables 5 and 6). This is easily explained by the decrease of the force constant of the C–S oscillator relative to the C–O one, due to the lower electronegativity of the S atom and the higher C–S bond length—135.8 (C_4–O_{13}) *vs.* 177.5 pm (C_4–S_{13}) and 142.2 (C_{14}–O_{13}) *vs.* 182.2 pm (C_{14}–S_{13}) (Tables 2 and 3). Furthermore, the vibrational modes assigned to the methyl group, particularly the symmetric deformations, are rather sensitive to the electronegativity of the attached atom (either O or S). Therefore, by replacing oxygen by sulfur the corresponding band at 1432 cm^{-1} is shifted to 1332 cm^{-1} (Tables 5 and 6). Also, the O → S substitution is responsible for the deviation of δ_{as} (CH_3) from 1469 to 1409 cm^{-1}. Moreover, it was verified that replacing O by S substitution causes an upward shift of ν_{as} (NO_2) (1298 to 1313 cm^{-1}) and a downward shift of δ_{as} $(CH_3)_{chain}$ (1469 to 1438 cm^{-1}).

These results suggest that π-electron delocalisation is more pronounced in 4-MeO-MeNS than in 4-MeS-MeNS, due to the electronegativity difference between the oxygen and sulfur atoms, this effect being very clearly reflected in the corresponding vibrational spectra, as discussed above.

A good overall agreement was obtained between the experimental and calculated frequency values, as well as between these results and data obtained by the authors for other nitrostyrenes derivatives,[14] namely *β*-methyl-*β*-nitrostyrene, the synthetic precursor of methamphetamine. Furthermore, the present results are in conformity with those previously reported for 2,5-dimethoxy-4-methyl-*β*-methyl-*β*-nitrostyrene (the precursor of 2,5-dimethoxy-4-methylamphetamine)[30] and similar systems.[31–38]

The present study allowed the assignment of specific vibrational features, characteristic of each of the *β*-methyl-*β*-nitrostyrenes investigated. Therefore, these results will be very useful for the identification of compounds present in illegally manufactured drugs of abuse, as well as for determining the corresponding synthetic routes and, hopefully, for tracking the clandestine laboratories where production takes place.

4 Conclusions

A complete conformational analysis was carried out for the synthetic precursors of amphetamine-like drugs 3,4-methylenedioxy-*β*-methyl-*β*-nitrostyrene (3,4-MD-MeNS), 4-methoxy-*β*-methyl-*β*-nitrostyrene (4-MeO-MeNS) and 4-methylthio-*β*-methyl-*β*-nitrostyrene (4-MeS-MeNS), by Raman spectroscopy combined to *ab initio* MO calculations.

Several distinct conformers were obtained for these compounds, varying in the orientation of the CH_3 and NO_2 groups relative to both the aromatic ring and the C_7=C_8 bond. A clear preference for a planar geometry was found in all cases, except when strong steric hindrance effects occurred in the planar conformations. In fact, the most stable geometries were found to be the ones allowing a more effective balance between the following parameters: π-electron delocalisation, minimisation of repulsive effects and formation of stabilising (C)H···O intramolecular close contacts. The results presently described are in very good accordance with the ones obtained in previous studies on similar *β*-nitrostyrene derivatives.

Despite their undisputable interest, the number of reported

Table 4 Raman experimental (solid state) and calculated (B3LYP/6-31G**) wavenumbers (cm^{-1}) for the most stable conformers of 3,4-MD-MeNS

	[a]Calculated		
Experimental	3,4-MD-MeNS 1	3,4-MD-MeNS 2	[b]Approximate description
3116	3128 (1;33)	3114 (2;76)	$\nu\ (CH)_{ring}$
3097	3105 (4;161)	3099 (4;95)	$\nu\ (CH)_{ring}$
3088	3079 (1;76)	3096 (1;47)	$\nu\ (CH)$
3065	3073 (3;10)	3071 (1;30)	$\nu\ (CH)$
3040	3041 (3;56)	3040 (3;55)	$\nu_{as}\ (CH_3)$
3027	3005 (8;75)	3004 (8;81)	$\nu_{as}\ (CH_3)$
2975	2980 (46;200)	2972 (43;202)	$\nu_{as}\ (CH_2)$
2938	2934 (10;174)	2935 (9;186)	$\nu_{s}\ (CH_3)$
2915	2917 (140;275)	2922 (150;299)	$\nu_{s}\ (CH_2)$
2860			$(1256 + 1604\ cm^{-1})$
2803			$(1308 + 1495\ cm^{-1})$
2759			$(1112 + 1647\ cm^{-1})$
2632			$2 \times \nu_{s}\ (NO_2)$
2616			$2 \times \nu\ (CC)_{ring}$
2582			$(1266 + 1316\ cm^{-1})$
2578			$(1256 + 1316\ cm^{-1})$
2368			$(1112 + 1256\ cm^{-1})$
1647	1644 (86;898)	1649 (61;621)	$\nu\ (C{=}C)_{chain}$
1619	1604 (39;553)	1602 (63;989)	$\nu\ (CC)_{ring}$
1604	1587 (21;188)	1591 (3;6)	$\nu\ (CC)_{ring}$
1495	1555 (146;113)	1556 (168;116)	$\nu_{as}\ (NO_2)$
	1503 (8;54)	1504 (8;59)	$\delta\ (CH_2)$ (sciss.)
	1479 (273;8)	1480 (312;5)	$\delta\ (CH)_{ring} + \delta\ (CH_2)$ (sciss.)
	1442 (4;49)	1443 (1;73)	$\delta_{as}\ (CH_3)$
1450	1438 (92;147)	1436 (45;58)	$\nu\ (CC)_{ring} + \delta_{as}\ (CH_3)$
1434	1431 (48;126)	1425 (46;58)	$\delta_{as}\ (CH_3)$
	1389 (1;37)	1389 (2;33)	$\omega\ (CH_2)$
	1385 (20;15)	1380 (35;55)	$\delta_{s}\ (CH_3) + \delta\ (CH)_{chain}$
1365	1350 (19;108)	1353 (10;25)	$\delta_{s}\ (CH_3) + \delta\ (CH)_{chain}$
	1319 (88;194)	1323 (12;4)	$\delta\ (CH)$
1316	1313 (386;936)	1311 (648;1515)	$\nu_{s}\ (NO_2) + \delta_{s}\ (CH_3)$
1308	1262 (645;299)	1263 (18;74)	$\nu\ (CC)_{ring}$
1266	1245 (2;4)	1248 (434;41)	$\delta\ (CH)$
1256	1190 (12;127)	1181 (1;57)	$\delta\ (CH)$
1201	1156 (1;13)	1154 (0;10)	$t\ (CH_2)$
1142	1121 (9;4)	1127 (2;4)	$\delta\ (CH)_{ring}$
	1100 (10;1)	1099 (10;1)	$r\ (CH_2)$
1112	1092 (68;174)	1086 (10;10)	$\delta\ (CC)$
1094	1077 (3;11)	1079 (63;131)	$\delta\ (CC)$
1034	1030 (126;1)	1030 (3;1)	$\delta\ (OCO) + \delta\ (CH)_{ring} + r\ (CH_3)$
	1025 (7;25)	1026 (1;25)	$r\ (CH_3)$
982	967 (72;30)	970 (64;21)	$r\ (CH_3)$
945	937 (35;2)	938 (37;13)	$\nu\ (C_{16}O)$
926	934 (17;100)	929 (42;160)	$\gamma\ (CH)_{chain}$
	912 (39;19)	907 (19;1)	$\delta\ (CC)_{ring}$
869	898 (3;6)	902 (21;7)	$\gamma\ (CH)_{ring}$
	845 (33;6)	844 (29;2)	$\gamma\ (CH)_{ring}$
830	840 (45;4)	837 (50;7)	$\delta\ (NO_2)$ (sciss.) $+ \gamma\ (CH)_{ring}$
	806 (8;16)	801 (17;7)	$\delta\ (CC)_{ring} + \delta\ (CO_{14}C)$
787	795 (25;5)	796 (17;21)	$\gamma\ (CH)_{ring}$
	768 (4;15)	768 (8;7)	$\gamma\ (CH)_{ring} + \delta\ (CO_8C)$
717	713 (6;2)	719 (2;0)	$\omega\ (NO_2) + \gamma\ (CCC)$
700	707 (1;23)	712 (8;1)	$\delta\ (COC)$
	689 (6;23)	695 (1;58)	$\gamma\ (CCC) + \nu\ (CN)$
625	678 (2;12)	679 (1;2)	$\gamma\ (CCC)_{ring}$
604	610 (5;4)	605 (1;8)	$\delta\ (CCC)$
550	590 (10;3)	593 (11;1)	$\gamma\ (CCC)_{ring}$
524	535 (9;9)	543 (8;1)	$\delta\ (CCC)_{ring}$
	516 (6;17)	518 (3;22)	$\delta\ (CNO)$
461	451 (8;34)	442 (10;21)	$\Delta\ (CCC)_{chain}$
439	429 (6;9)	411 (9;4)	$\Delta(CCC)_{ring}$
405	401 (3;10)	406 (2;13)	$\Delta\ (CCN)$
	386 (1;0)	389 (1;1)	$\Gamma(CCC)$
	351 (1;2)	353 (2;4)	$\Gamma\ (CCC)$
303	300 (5;3)	290 (2;1)	$\tau\ (CH_3)$
230	259 (0;2)	249 (1;3)	$\Gamma\ (CCC)_{ring}$
207	229 (1;3)	242 (0;7)	$\Gamma\ (CCC)$
147	200 (0;4)	206 (1;1)	Skeletal mode
115	179 (0;2)	183 (0;3)	$\tau\ (CH_3)$
	100 (1;0)	103 (1;3)	$\tau\ (CH_3)$
77	75 (4;1)	71 (1;2)	Skeletal mode
58	63 (5;3)	61 (2;1)	Skeletal mode

Table 4 Raman experimental (solid state) and calculated (B3LYP/6-31G**) wavenumbers (cm^{-1}) for the most stable conformers of 3,4-MD-MeNS (*Continued*)

	[a]Calculated		
Experimental	3,4-MD-MeNS 1	3,4-MD-MeNS 2	[b]Approximate description
	48 (3;2)	36 (0;3)	Skeletal mode
	37 (0;3)	15 (7;1)	Skeletal mode

[a] B3LYP/6-31G** level; wavenumbers above 400 cm^{-1} are scaled by 0.9614 [28] (IR intensities in km mol^{-1}; Raman scattering activities in Å amu^{-1}). [b] Atoms are numbered according to Fig. 2.; δ and γ stand for in-plane and out-of-plane deformations, respectively; Δ and Γ stand for in-plane and out-of-plane skeletal deformations, respectively.

Table 5 Raman experimental (solid state) and calculated (B3LYP/6-31G**) wavenumbers (cm^{-1}) for the most stable conformers of 4-MeO-MeNS

	[a]Calculated		
Experimental	4-MeO-MeNS 1	4-MeO-MeNS 2	[b]Approximate description
3107	3107 (3;92)	3108 (7;87)	$\nu\ (CH)_{ring}$
	3103 (12; 86)	3094 (2;73)	$\nu\ (CH)_{ring}$
3083	3087 (4;90)	3093 (10;113)	$\nu\ (CH)_{ring}$
3076	3072 (0;52)	3072 (0;59)	$\nu\ (CH)_{chain}$
3055	3065 (7;30)	3066 (6;30)	$\nu\ (CH)$
3045	3040 (3;60)	3039 (3;59)	$\nu_{as}\ (CH_3)_{chain}$
3033	3036 (22;156)	3036 (23;159)	$\nu_{as}\ (CH_3)_{ring}$
3007	3003 (8;76)	3002 (8;75)	$\nu_{as}\ (CH_3)_{chain}$
2976	2971 (36;64)	2970 (36;56)	$\nu_{as}\ (CH_3)_{ring}$
2944			$(1298 + 1646\ cm^{-1})$
2928	2933 (10;182)	2933 (10;170)	$\nu_{s}\ (CH_3)_{chain}$
2907	2907 (65;137)	2906 (59;125)	$\nu_{s}\ (CH_3)_{ring}$
2782			$(1177 + 1605\ cm^{-1})$
2610			$(1298 + 1312\ cm^{-1})$
2596			$2 \times \nu_{s}\ (NO_2)$
2554			$(1256 + 1298\ cm^{-1})$
2526			$(921 + 1605\ cm^{-1})$
2474			$(1218 + 1256\ cm^{-1})$
1646	1644 (63;837)	1645 (57;723)	$\nu\ (C{=}C)_{chain}$
1605	1600 (262;1062)	1599 (270;1145)	$\nu\ (CC)_{ring}$
1516	1550 (28;53)	1551 (16;4)	$\nu\ (CC)_{ring}$
1495	1554 (155;125)	1555 (147;123)	$\nu_{as}\ (NO_2)$
1476	1500 (97;47)	1499 (98;45)	$\nu\ (CC)_{ring}$
	1458 (40;13)	1458 (49;16)	$\delta_{as}\ (CH_3)_{ring}$
1469	1448 (6;31)	1447 (6;30)	$\delta_{as}\ (CH_3)_{ring}$
1452	1441 (9;38)	1442 (5;37)	$\delta_{as}\ (CH_3)_{chain}$
	1433 (18;18)	1432 (15;17)	$\delta_{as}\ (CH_3)_{chain} + \delta_{s}\ (CH_3)_{ring}$
1432	1431 (13;5)	1432 (15;9)	$\delta_{s}\ (CH_3)_{ring}$
	1411 (13;39)	1409 (2;1)	$\delta\ (CH) + \delta_{s}\ (CH_3)_{chain}$
1387	1382 (28;17)	1382 (31;20)	$\delta_{s}\ (CH_3)_{chain}$
1355	1340 (27;99)	1340 (4;59)	$\delta_{s}\ (CH_3)_{chain} + \delta\ (CH)_{chain}$
1298	1313 (401;974)	1316 (213;479)	$\nu_{s}\ (NO_2) + \delta\ (CH)$
1312	1303 (62;16)	1302 (466;834)	$\nu\ (CC)_{ring}$
	1289 (30;107)	1292 (2;40)	$\delta\ (CH)_{ring}$
1256	1258 (583;217)	1258 (386;45)	$\nu\ (C_4O + \delta_{s}\ (CH_3)_{chain} + \delta\ (CH)$
1218	1208 (15;216)	1205 (25;148)	$\delta\ (CH)_{ring}$
	1164 (7;6)	1164 (21;19)	$r\ (CH_3)_{ring}$
1177	1161 (137;193)	1159 (115;179)	$\delta\ (CH)_{ring}$
1123	1132 (1;5)	1132 (1;5)	$r\ (CH_3)_{ring}$
1105	1106 (6;3)	1106 (16;11)	$\delta\ (CH)_{ring}$
	1079 (30;68)	1080 (25;62)	$r\ (CH_3)_{chain} + \delta\ (CH)_{chain}$
1037	1030 (60;1)	1030 (59;1)	$\nu\ (C_{14}O)$
	1026 (1;23)	1026 (1; 25)	$r\ (CH_3)_{chain}$
984	986 (5;3)	987 (4;2)	$\delta\ (CC)_{ring}$
964	963 (91;26)	963 (89;23)	$r\ (CH_3)_{chain}$
951	939 (16;76)	942 (17;76)	$\omega_{as}\ (CH)_{ring} + \gamma\ (CH)_{chain}$
922	934 (8;23)	926 (6;26)	$\omega_{as}\ (CH)_{ring}$
875	912 (6;20)	919 (10;30)	$\omega_{as}\ (CH)_{ring} + \gamma\ (CH)_{chain}$
846	853 (47;17)	853 (45;18)	$\delta\ (NO_2)\ (sciss.) + \delta\ (CC)_{ring}$
829	824 (42;9)	825 (37;11)	$\omega_{s}\ (CH)_{ring}$
812	811 (25;40)	810 (28;29)	$\omega_{s}\ (CH)_{ring}$
780	794 (7;4)	794 (8;15)	$\omega_{as}\ (CH)_{ring}$
	752 (5;13)	759 (1;13)	$\delta\ (CC)$
716	718 (5;0)	718 (4;0)	$\omega\ (NO_2) + \gamma\ (CC)_{ring}$
694	698 (8;20)	696 (10;14)	$\gamma\ (CC)_{ring} + \omega\ (NO_2)$
	682 (3;11)	677 (3;12)	$\gamma\ (CC)_{ring} + \delta\ (CC)_{chain}$
633	621 (0;6)	622 (1;7)	$\delta\ (CC)_{ring}$

Table 5 Raman experimental (solid state) and calculated (B3LYP/6-31G**) wavenumbers (cm^{-1}) for the most stable conformers of 4-MeO-MeNS (*Continued*)

Experimental	[a]Calculated		[b]Approximate description
	4-MeO-MeNS 1	4-MeO-MeNS 2	
560	547 (22;2)	545 (26;10)	δ (COC)
528	529 (13;2)	527 (17;1)	γ $(CC)_{ring}$
	520 (5;16)	513 (7;12)	γ $(CC)_{ring}$
476	449 (2;1)	464 (2;17)	δ (COC) + δ $(CC)_{chain}$
445	438 (13;54)	436 (8;30)	γ $(CC)_{chain}$
425	413 (0;1)	414 (2;5)	γ $(CC)_{ring}$
	389 (1;1)	387 (1;0)	Δ (CCN) + Γ (CCC)
351	355 (3;1)	358 (3;2)	Γ (CCC)
	340 (5;1)	325 (0;3)	Δ $(CCC)_{chain}$ + Δ (COC)
277	253 (0;1)	271 (3;1)	τ (CH_3)
	239 (0;1)	251(0;1)	τ $(CH_3)_{ring}$
	236 (0;1)	219 (2;4)	τ $(CH_3)_{chain}$
	196 (0;1)	194 (0;1)	τ (CH_3)
130	173 (0;5)	184 (0;4)	τ $(CH_3)_{chain}$
114	110 (4;3)	111 (5;2)	Skeletal mode
	101 (3;1)	101 (1;1)	Skeletal mode
75	65 (1;2)	66 (1;3)	Skeletal mode
	56 (1;1)	51 (0;0)	Skeletal mode
	37 (0;3)	41 (0;4)	Skeletal mode

[a] B3LYP/6-31G** level; wavenumbers above 400 cm^{-1} are scaled by 0.9614 [28] (IR intensities in km mol^{-1}; Raman scattering activities in Å amu^{-1}). [b] Atoms are numbered according to Fig. 2.; δ and γ stand for in-plane and out-of-plane deformations, respectively; Δ and Γ stand for in-plane and out-of-plane skeletal deformations, respectively.

Table 6 Raman experimental (solid state) and calculated (B3LYP/6-31G**) wavenumbers (cm^{-1}) for the most stable conformers of 4-MeS-MeNS

Experimental	[a]Calculated		[b]Approximate description
	4-MeS-MeNS 1	4-MeS-MeNS 2	
3174	3104 (4;65)	3151 (5;39)	ν $(CH)_{ring}$
3093	3098 (10;74)	3099 (9;82)	ν $(CH)_{ring}$
3079	3072 (0;55)	3093 (7;157)	ν $(CH)_{chain}$
	3067 (2;85)	3059 (12;68)	ν (CH)
	3063 (8;21)	3036 (23;164)	ν (CH)
3047	3041 (3;62)	3031 (17;78)	ν_{as} $(CH_3)_{chain}$
	3039 (3;145)	3021 (4;38)	ν_{as} $(CH_3)_{ring}$
	3029 (7;58)	2998 (10;129)	ν_{as} $(CH_3)_{ring}$
3003	3004 (8;82)	2974 (34;55)	ν_{as} $(CH_3)_{chain}$
2987	2944 (18;169)	2940 (20;310)	ν_{s} $(CH_3)_{ring}$
2926	2934 (9;202)	2909 (60;131)	ν_{s} $(CH_3)_{chain}$
2745			(1195 + 1650 cm^{-1})
2612			2 × ν_{s} (NO_2)
2502			(1196 + 1306 cm^{-1})
2401			(1095 + 1306 cm^{-1})
2393			2 × δ $(CH)_{ring}$
1650	1645 (87;1317)	1630 (62;425)	ν (C = C)$_{chain}$
1641	1586 (177;1848)	1596 (448;1089)	ν $(CC)_{ring}$
1587	1556 (155;170)	1554 (11;9)	ν_{as} (NO_2)
1547	1532 (8;66)	1535 (98;126)	ν $(CC)_{ring}$
1509	1479 (38;22)	1497 (97;51)	ν $(CC)_{ring}$ + δ $(CH)_{ring}$
1468	1441 (26;10)	1458 (51;15)	δ_{as} $(CH_3)_{ring}$
1438	1440 (12;43)	1449 (14;12)	δ_{as} $(CH_3)_{chain}$
	1432 (16;19)	1447 (6;31)	δ_{as} (CH_3) $_{chain}$
1409	1426 (10;30)	1432 (13;9)	δ_{as} $(CH_3)_{ring}$
1389	1398 (21;30)	1425 (6;19)	ν $(CC)_{ring}$ + δ_{s} $(CH_3)_{ring}$
	1382 (21;17)	1412 (9;28)	δ_{s} $(CH_3)_{chain}$ + δ (CH)
1360	1338 (23;164)	1382 (25;219)	δ_{s} $(CH_3)_{chain}$ + δ $(CH)_{chain}$
1334	1322 (1;21)	1366 (51;76)	δ_{s} $(CH_3)_{ring}$
1313	1292 (63;283)	1299 (163;265)	ν $(CC)_{ring}$
1306	1313 (599;1515)	1319 (249;477)	ν_{s} (NO_2) + δ_{s} $(CH_3)_{chain}$ + δ (CH)
	1280 (9;17)	1289 (11;22)	ν $(CC)_{ring}$
1225	1210 (20;222)	1261 (374;74)	ν $(CC)_{ring}$ + δ $(CH)_{ring}$
1196	1177 (29;315)	1203 (59;209)	δ $(CH)_{ring}$
	1115 (4;2)	1165 (41;31)	δ $(CH)_{ring}$
1124	1080 (10;45)	1164 (191;171)	δ $(CC)_{chain}$ + δ (CH)
1095	1070 (144;408)	1131 (1;4)	ν (C_4S)
1037	1026 (0;33)	1126 (30;22)	r $(CH_3)_{chain}$
982	991 (2;3)	1100 (14;13)	δ $(CC)_{ring}$
964	963 (83;67)	1032 (7;5)	r (CH_3) + δ (CH) $_{chain}$
	957 (20;12)	1031 (52;1)	r $(CH_3)_{ring}$
	945 (1;15)	999 (41;7)	r $(CH_3)_{ring}$ + γ $(CH)_{chain}$ + ω_{as} $(CH)_{ring}$

Table 6 Raman experimental (solid state) and calculated (B3LYP/6-31G**) wavenumbers (cm^{-1}) for the most stable conformers of 4-MeS-MeNS (*Continued*)

Experimental	[a]Calculated		[b]Approximate description
	4-MeS-MeNS 1	4-MeS-MeNS 2	
948	941 (16;78)	985 (3;1)	r $(CH_3)_{ring}$ + γ $(CH)_{chain}$ + ω_{as} $(CH)_{ring}$
	936 (8;36)	945 (2;6)	γ $(CH)_{chain}$ + ω_{as} $(CH)_{ring}$
920	918 (9;61)	932 (2;9)	γ $(CH)_{chain}$ + ω_{as} $(CH)_{ring}$
875	851 (48;14)	897 (15;27)	δ (NO_2) (sciss.) + δ $(CC)_{ring}$
820	813 (36;6)	863 (28;7)	ω_s $(CH)_{ring}$
	808 (0;17)	824 (24;38)	ω_{as} $(CH)_{ring}$
735	793 (25;14)	812 (29;23)	ω_s $(CH)_{ring}$
716	719 (0;4)	793 (0;5)	ω (NO_2) + γ $(CC)_{ring}$
	710 (6;13)	757 (4;2)	ω (NO_2) + δ $(CC)_{chain}$
662	694 (6;24)	736 (15;9)	ν $(C_{14}S)$ + γ $(CC)_{ring}$
	683 (4;7)	698 (1;2)	γ $(CC)_{ring}$
632	643 (1;17)	646 (1;12)	γ $(CC)_{ring}$
	620 (0;7)	608 (4;6)	δ $(CC)_{ring}$
537	524 (6;16)	579 (11;3)	δ (CCN)
518	506 (15;28)	517 (5;5)	γ (CC)
461	450 (2;4)	510 (28;14)	γ (CC)
435	424 (19;63)	465 (2;3)	γ $(CC)_{chain}$
	405 (0;2)	422 (7;16)	δ $(CC)_{ring}$
	381 (1;2)	404 (0;0)	Δ (CCN)
361	361 (1;5)	376 (1;2)	Δ (CCC) + Δ (CSC)
	331 (1;1)	354 (3;3)	Γ (CCC)
314	314 (4;5)	299 (5;1)	Δ (CCC) + Δ (CSC)
	230 (0;1)	276 (0;4)	τ $(CH_3)_{ring}$
218	222 (1;0)	252 (1;1)	τ (CH_3)
	204 (0;0)	224 (0;2)	τ $(CH_3)_{chain}$
	170 (0;0)	209 (0;1)	τ $(CH_3)_{chain}$
118	159 (0;8)	190 (3;1)	τ $(CH_3)_{chain}$
82	97 (2;5)	139 (1;1)	Skeletal mode
	64 (1;4)	114 (2;1)	Skeletal mode
	56 (4;2)	62 (3;2)	Skeletal mode
	50 (0;2)	34 (3;6)	Skeletal mode
	31 (1;3)	27 (1;1)	Skeletal mode

[a] B3LYP/6-31G** level; wavenumbers above 400 cm^{-1} are scaled by 0.9614 [28] (IR intensities in km mol^{-1}; Raman scattering activities in Å amu^{-1}). [b] Atoms are numbered according to Fig. 2, irrespective of the type of atom (O or S); δ and γ stand for in-plane and out-of-plane deformations, respectively; Δ and Γ stand for in-plane and out-of-plane skeletal deformations, respectively.

studies aiming at the identification of synthetic precursors of drugs of abuse by vibrational spectroscopy methods is very scarce. The present work intends to develop this field of research. In fact, the described results allow us to evaluate Raman spectroscopy, enabling rapid and non-destructive measurements, as a most promising tool for Forensic Sciences, as a screening method for the determination of the composition profiles of illicit substances, as well as for tracking clandestine laboratories. Actually, it was shown that even chemically similar intermediates are easily distinguished by this technique. It can also surpass other analytical methods currently used in criminal prosecutions once it allows the concomitant identification of both the active compound and its by-products. The method has the additional advantage of permitting its extension to the main metabolites of the amphetamine-like drugs presently investigated.

Although analysis of multiple illicit preparations will still need to be carried out, in order to ensure reproducibility of the technique, it will hopefully be possible, in the near future, to rely on a Raman database that will constitute an invaluable tool, for both forensic control and toxicological studies.

Acknowledgements

N. Milhazes is grateful to FCT for a fellowship (PRAXIS XXI/BD/18520/98). Thanks are also due to Laboratório Associado CICECO (University of Aveiro, Portugal) for access to the FT-Raman spectrometer, and to Ana M. Amado, for obtaining these spectra.

References

1 A. G. M. Barret and G. Graboski, *Chem. Rev.*, 1986, **86**, 751.
2 G. W. Kabalka, L. H. M. Guindi and R. S. Varma, *Tetrahedron*, 1990, **46**(21), 7443.
3 A. García-Torres, R. Cruz-Almanza and L. D. Miranda, *Tetrahedron Lett.*, 2004, **45**, 2085.
4 C. F. Yao, W. C. Chen and Y. M. Lin, *Tetrahedron Lett.*, 1996, **37**(35), 6339.
5 M. Schmidt and K. Eger, *Pharmazie*, 1996, **51**, 11.
6 T. A. Dal Cason, *J. Forensic Sci.*, 1990, **35**(3), 675.
7 K. C. Carter, Y. S. Finnon, N. Nic-Daeid, D. C. Robson and R. Waddell, *Immunopharmacol. Immunotoxicol.*, 2002, **24**(2), 187.
8 A. J. Poortman and E. Lock, *J. Forensic Sci. Int.*, 1999, **100**(3), 221.
9 S. E. J. Bell, D. T. Burns, A. C. Dennis and J. S. Speers, *Analyst*, 2000, **125**, 541.
10 S. E. J. Bell, D. T. Burns, A. C. Dennis, L. J. Matchett and J. S. Speers, *Analyst*, 2000, **125**, 1811.
11 B. Sägmüller, B. Schwarze, G. Brehm and S. Schneider, *Analyst*, 2001, **126**, 2066.
12 K. Faulds, W. E. Smith, D. Graham and R. J. Lacey, *Analyst*, 2002, **127**, 282.
13 T. Vankeirsbilck, A. Vercauteren, W. baeyens, G. van der Weken, F. Verpoort, G. Vergote and J. P. Remon, *Trends Anal. Chem.*, 2002, **21**, 869.
14 R. Calheiros, N. Milhazes, F. Borges and M. P. M. Marques, *J. Mol. Struct.*, 2004, **692**, 91.
15 M. J. Frisch, *et al.*, *Gaussian 98, Revision A.9*, Gaussian Inc., Pittsburgh PA, USA, 1998.
16 T. V. Russo, R. L. Martin and P. J. Hay, *J. Phys. Chem.*, 1995, **99**, 17085.
17 A. Ignaczak and J. A. N. F. Gomes, *Chem. Phys. Lett.*, 1996, **257**, 609.
18 F. A. Cotton and X. Feng, *J. Am. Chem. Soc.*, 1997, **119**, 7514.

19 A. Ignaczak and J. A. N. F. Gomes, *J. Electroanal. Chem.*, 1997, **420**, 209.
20 T. Wagener and G. Frenking, *Inorg. Chem.*, 1998, **37**, 1805.
21 F. A. Cotton and X. Feng, *J. Am. Chem. Soc.*, 1998, **120**, 3387.
22 C. Lee, W. Yang and R. G. Parr, *Phys. Rev.*, 1988, **B37**, 785.
23 B. Miehlich, A. Savin, H. Stoll and H. Preuss, *Chem. Phys. Lett.*, 1989, **157**, 200.
24 A. D. Becke, *Phys. Rev.*, 1988, **A38**, 3098.
25 A. D. Becke, *J. Chem. Phys.*, 1993, **98**, 5648.
26 P. C. Hariharan and J. A. Pople, *Theor. Chim. Acta*, 1973, **28**, 213.
27 M. M. Francl, W. J. Pietro, W. J. Hehre, J. S. Binkley, M. S. Gordon, D. J. DeFrees and J. A. Pople, *J. Chem. Phys.*, 1982, **77**, 3654.
28 A. P. Scott and L. Radom, *J. Phys. Chem.*, 1996, **100**, 16502.
29 C. Peng, P. Y. Ayala, H. B. Schlegel and M. J. Frisch, *J. Comput. Chem.*, 1996, **17**, 49.
30 A. By, G. Neville and H. F. Shurvell, *J. Forensic Sci.*, 1992, **37**, 503.
31 R. E. Clavijo, R. Araya-Maturana, B. K. Cassels and B. Weiss-López, *Spectrochim. Acta, Part A*, 1996, **50**(12), 2105.
32 F. J. Ramírez and J. T. López Navarrete, *Vib. Spectrosc.*, 1993, **4**, 321.
33 R. Hargitai, P. G. Szalay, G. Pongor and G. Fogarasi, *J. Mol. Struct. (THEOCHEM)*, 1994, **306**, 293.
34 Y. Haas, S. Kendler, E. Zingher, H. Zuckermann and S. Zilberg, *J. Chem. Phys.*, 1995, **103**, 37.
35 S. J. Greaves and W. W. Griffith, *Spectrochim. Acta, Part A*, 1991, **47**, 133.
36 M. Gerhards, W. Perl, S. Schumm, U. Henrichs, C. Jacoby and K. Kleinermanns, *J. Chem. Phys.*, 1996, **104**, 9362.
37 S. M. Fiuza, E. Besien, N. Milhazes, F. Borges and M. P. M. Marques, *J.Mol. Struct.*, 2004, **693**(1–3), 103–118.
38 E. Besien and M. P. M. Marques, *J. Mol. Struct. (THEOCHEM)*, 2003, **625**, 265.